DAMPING OF THE SECOND MODE INSTABILITY ON A CONE IN HYPERSONIC FLOW

Sebastian Willems and Ali Gülhan

German Aerospace Center (DLR), Institute of Aerodynamics and Flow Technology, Supersonic and Hypersonic Technology Department, Linder Höhe, 51147 Köln, Germany, sebastian.willems@dlr.de

ABSTRACT

This paper presents the results of transition experiments with a 3° half angle cone at Mach 6. The transition position was measured with an infrared camera and simultaneously the pressure fluctuations in the boundary layer with high speed pressure sensors. A segment with regular micro pores causes a measurable damping of the pressure fluctuations in the boundary layer (Mack modes) but no transition delay. In addition the influence of the nose radius, of the unit Reynolds number and of the free stream temperature on the transition as well as the pressure fluctuations is investigated.

Key words: transition; Mack mode; damping; slender cone.

1. INTRODUCTION

The transition from a laminar to a turbulent boundary layer is attended by an increase of the heat flux and drag. An aim of the design of hypersonic vehicles is therefore to delay the transition as long as possible. In hypersonic flows over smooth surfaces the transition is most likely provoked by first and second mode instabilities. As the first modes (Tollmien-Schlichting waves) can be damped by cooled structures, the second modes (Mack modes) become dominant and their damping is the topic of several research projects. Rasheed et al. [5] could demonstrate a damping of these trapped acoustic waves and a delay of the transition on a 5° half cone with a regular porous surface at Mach 5. Fedorov et al. [2] verified the damping of the Mack mode with a 7° half cone and a porous coating of random micro structures at Mach 6.

New transition experiments with a 3° half angle cone at Mach 6 were performed in the hypersonic wind tunnel (H2K) of the German Aerospace Center (DLR) in Cologne. The used model is equipped with PCB high speed pressure sensors and the main parts are made of polyether ether ketone (PEEK). Therefore simultaneous measurements of the transition position with an infrared camera and the pressure fluctuations in the boundary layer are possible. The dimensions of the micro pores drilled in the surface of one module base on the calculations of Wartemann et al. [9]. They cause a measurable damping of the pressure fluctuations in the boundary layer. The influence of the nose radius is investigated with the help of exchangeable metal apexes. In addition the operating map of the H2K allows an examination of the effect of the unit Reynolds number and of the free stream temperature.

Figure 1. Test section of the H2K with the cone model

The objective of this paper is a more detailed investigation of the dependencies of the Mack mode including the damping with a regular porous surface.

2. EXPERIMENTAL APPARATUS

2.1. Wind tunnel

The experiments were performed in the Hypersonic wind tunnel Cologne (H2K) [4]. It is a blowdown wind tunnel with a free jet test section and a test time of 30 s. Figure 1 shows the test section with the model. For the experiments a Mach 6 contour nozzle with an exit diameter of 600 mm was used. The inflowing air is heated with resistance heaters.

Proc. of '7th European Symposium on Aerothermodynamics', Brugge, Belgium 9–12 May 2011 (ESA SP-692, August 2011)

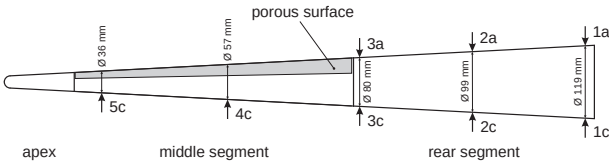

Figure 2. Sketch of the model parts

2.2. Model

The basic model shape is a 3° half angle cone with a base radius of 60.1 mm. The model consists of three exchangeable segments - the apex, the middle segment and the rear segment, see also figure 2. The steel apexes have nose radii of < 0.15 mm, 1 mm, 5 mm, 10 mm and 15 mm. Therefore the model length varies between 1146 mm and 877 mm. Two middle segments made of PEEK are in use – one with a plain surface and one with a generic porous surface formed by regular uniform blind holes. The holes are 80 μm in diameter, at least 1000 μm in depth and placed every 200 μm, thus the porosity is 12.6 %. A close-up is shown in figure 3. The choice of the hole dimensions base on simulations from Wartemann with NOLOT [9] [8] and the technical feasibility. The Fraunhofer Institute for Laser Technology (ILT) in Aachen performed the manufacturing of these holes with the help of laser drilling [7] using a pulsed INNOSLAB laser. In circumferential direction on third (120°) of the surface is perforated. The perforated area starts at a radius of 15.5 mm and ends at a radius of 39.5 mm, thus the porous area has a length of 456 mm and contains about 660 000 holes. The rear segment of the cone is also made of PEEK. The model is supported by a central steel shaft.

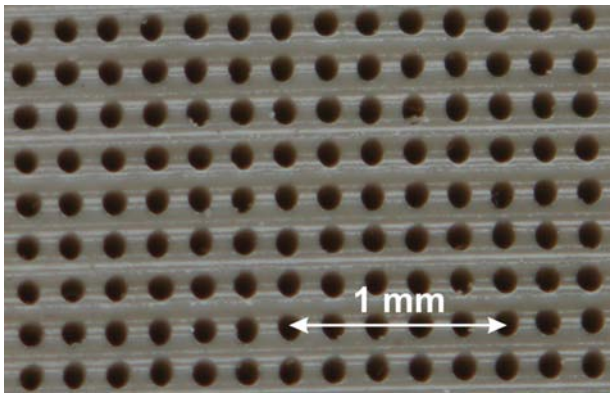

Figure 3. Close-up of the porous surface

2.3. Instrumentation

The surface temperature on the PEEK segments is captured via a FLIR SC3000 infrared camera [3]. The model is equipped with four kulite XCQ-080 sensors with a 35 kPa range and a natural frequency of 150 kHz for static and low speed surface pressure measurements. They are connected to a NI PXIe-4331 bridge module. For high speed

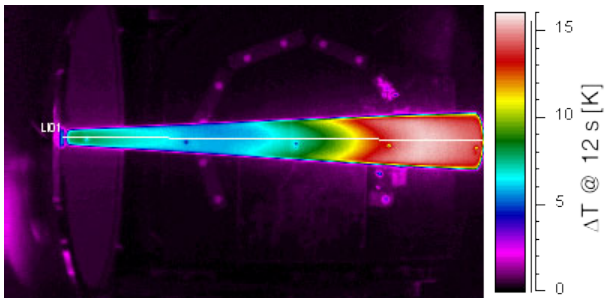

Figure 4. Surface temperature increase @ $Ma = 6.0$, $r_N = 0.15$, $Re = 4 \cdot 10^6 \frac{1}{\mathrm{m}}$, $T_0 = 500$ K, plain

pressure measurements the model is equipped with eight PCB 132A31 sensors (their positions are marked in figure 2) with a 350 kPa range and a resonant frequency above 1 MHz. They are connected to charge amplifiers PCB 482C05 and their output signals are measured with Adlink PXI-9816D/512 digitizers.

2.4. Data preparation

The raw data of the infrared camera are transferred into surface temperatures using ThermaCAM Researcher 2001. Then the temperature values along the symmetry line of the model are extracted. Afterwards the values of the last picture before the wind tunnel start is subtracted from the values 12 s later. The X-coordinates are transformed into the path length from the apex which splits into the arc length and the generatrix. With equation (1) the path length l on a cone with the half angle α (here $\alpha = \frac{\pi}{60}$) and the nose radius r_N can be calculated based on the cone radius r_B at this position.

$$l = \frac{r_B}{\sin(\alpha)} - \frac{r_N}{\tan(\alpha)} + r_N \cdot \left(\frac{\pi}{2} - \alpha\right) \qquad (1)$$

The frequency spectra of the PCB sensors, shown in this paper, base on measurements with a sampling rate of 4 MHz and a measurement period at stable flow conditions of 15 s. The gained data are divided into 5999 blocks with 20 000 samples each. The blocks overlap each other by 50 %. Each block is multiplied with the Hann function and afterwards Fourier transformed. The arithmetic mean of all block results is then scaled with the static pressure of the inflow. The frequency spectra show root mean square values.

3. RESULTS

3.1. Reynolds number

Figure 5 shows the temperature increase on the plain PEEK segments of the cone with a nose radius of 0.15 mm for three different Reynolds numbers. The transition region can be located with the help of the typical increase

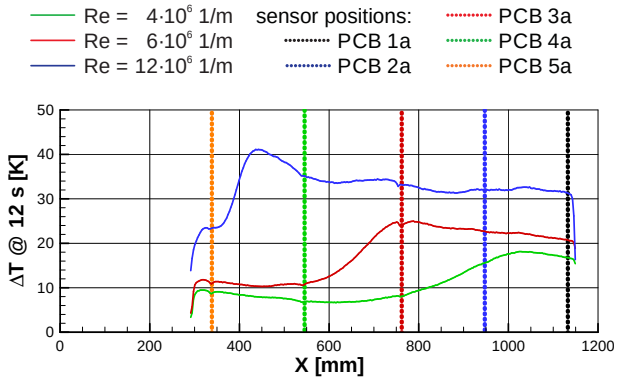

Figure 5. Surface temperature increase dependent on Reynolds number @ $Ma = 6.0$, $r_N = 0.15\,\mathrm{mm}$, $T_0 = 500\,\mathrm{K}$, plain

of the surface temperature. For a Reynolds number of $4 \cdot 10^6\,\frac{1}{\mathrm{m}}$ the transition takes place at a path length of 620 to 1020 mm, for $6 \cdot 10^6\,\frac{1}{\mathrm{m}}$ at 500 to 750 mm and for $12 \cdot 10^6\,\frac{1}{\mathrm{m}}$ at 340 to 440 mm. Thus with an increasing Reynolds number the length of the transition region decreases and moves upstream.

The pressure frequency spectra are shown in the figures 6(a)-(c). Their positions are also marked in figure 5. The significant peak at 50 kHz is no flow phenomenon as it appears also at reference measurements in vacuum. Nevertheless, the peaks of the Mack mode are quite obvious and its increase and destruction can be observed.

For the case with a Reynolds number of $4 \cdot 10^6\,\frac{1}{\mathrm{m}}$ (fig. 6(a)) there is nothing interesting in the spectrum of the first sensor (PCB 5c) at a path length of 339 mm. At a path length of 545 mm, this is still before the transition, the sensor 4c registers a small peak at 100 kHz. At a path length of 762 mm (PCB 3c), this is at the beginning of the transition, supposable the same peak has increased to 10% of the static pressure and moved to a frequency of 80 kHz. In addition a second smaller peak has formed at a frequency of 160 kHz. At a path length of 947 mm (PCB 2c), this is towards the end of the transition, the peak disappeared almost completely. There is just a small bump at 75 kHz. The frequency spectrum of the last sensor (PCB 5c) at a path length of 1133 mm is again completely even.

The situation for the two other Reynolds numbers is similar, but some differences are noticeable. As indicated by the temperature profiles, all effects move upstream. With a Reynolds number of $6 \cdot 10^6\,\frac{1}{\mathrm{m}}$ (fig. 6(b)) the first peak of the Mack modes is registered by PCB 5c and the biggest peak by PCB 4c. PCB 3c which is at the end of the transition region measures a broad increase of the pressure amplitudes for frequencies below 300 kHz. In comparison to the $6 \cdot 10^6\,\frac{1}{\mathrm{m}}$ case the frequency of the Mack mode at the same path lengths increases (175 kHz at PCB 5c and 125 kHz at PCB 4c). The reduced maximum amplitude and the hardly detectable second peak are not significant, as they highly depend on the sensor position in

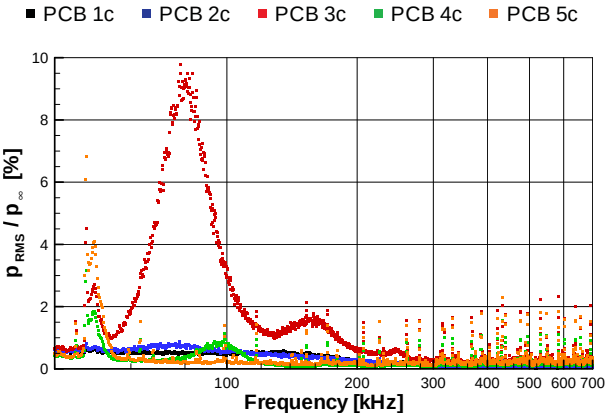

(a) $Re = 4 \cdot 10^6\,\frac{1}{\mathrm{m}}$

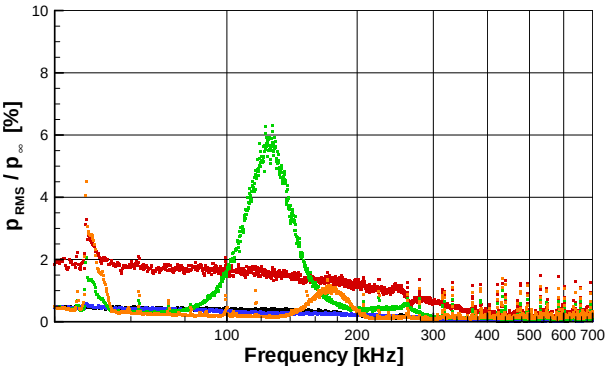

(b) $Re = 6 \cdot 10^6\,\frac{1}{\mathrm{m}}$

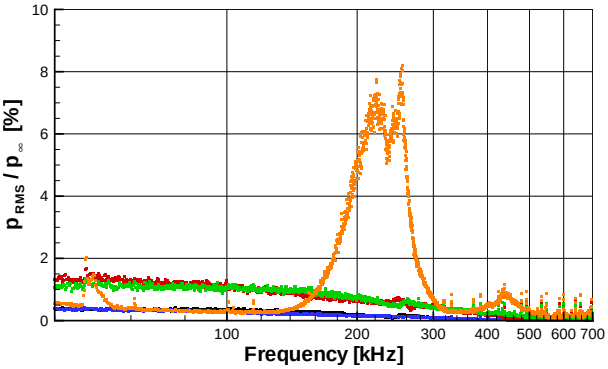

(c) $Re = 12 \cdot 10^6\,\frac{1}{\mathrm{m}}$

Figure 6. Pressure frequency spectra dependent on sensor position @ $Ma = 6.0$, $r_N = 0.15\,\mathrm{mm}$, $T_0 = 500\,\mathrm{K}$, plain

relation to the transition position. At a Reynolds number of $12 \cdot 10^6 \frac{1}{\mathrm{m}}$ the maximum amplitude of the second Mack mode is registered from PCB 5c at a still higher frequency around 240 kHz. In addition there is again a distinctive second peak at 440 kHz. This time PCB 4c and 3c measure a broad increase of the pressure amplitudes for frequencies below 300 kHz. The reduced noise level at higher Reynolds number is caused by the higher pressure level.

3.2. Nose radius

Figure 7 shows the temperature increase on the plain cone for several nose radii. The observed region of the PEEK segments shifts regarding the path length, because of the different length of the nose segments. It is obvious that the smaller the nose radius the earlier and the shorter is the transition region.

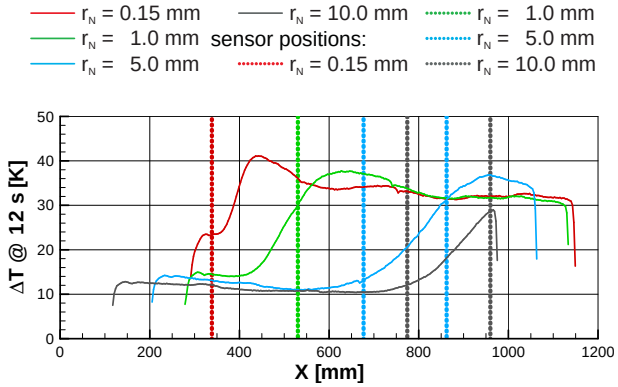

Figure 7. Temperature increase dependent on nose radius @ $Ma = 6.0$, $Re = 12 \cdot 10^6 \frac{1}{\mathrm{m}}$, $T_0 = 500\,\mathrm{K}$, plain

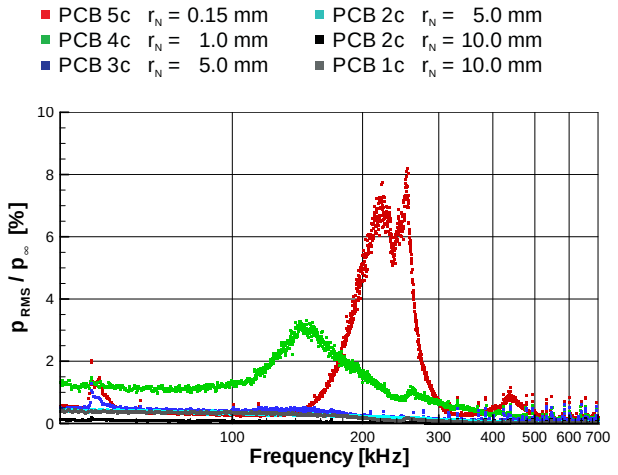

Figure 8. Pressure frequency spectra dependent on nose radius @ $Ma = 6.0$, $Re = 12 \cdot 10^6 \frac{1}{\mathrm{m}}$, $T_0 = 500\,\mathrm{K}$, plain

Due to the different nose lengths and the different transition positions a comparison of the pressure frequency spectra is difficult. The pressure frequency spectra of the positions marked in figure 7 are shown in figure 8. With a nose radius of 0.15 mm PCB 5c at the beginning of the transition region registers the already described conspicuous peak. With a nose radius of 1 mm PCB 4c in the middle of the transition region registers a smaller, less sharp peak at a lower frequency of 150 kHz but with a distinctive second peak at 260 kHz. For a nose radius of 5 mm as well as for 10 mm neither at the beginning of the transition region (PCB 3c respectively PCB 2c) nor at the end of the transition region (PCB 2c respectively PCB 1c) there are any noticeable peaks.

3.3. Temperature

Figure 9 shows, that a change of the temperature level with the same Reynolds number has no effect on the transition position. But figure 12 shows, that with the increasing temperature the frequency and the amplitude of the measured Mack mode increase.

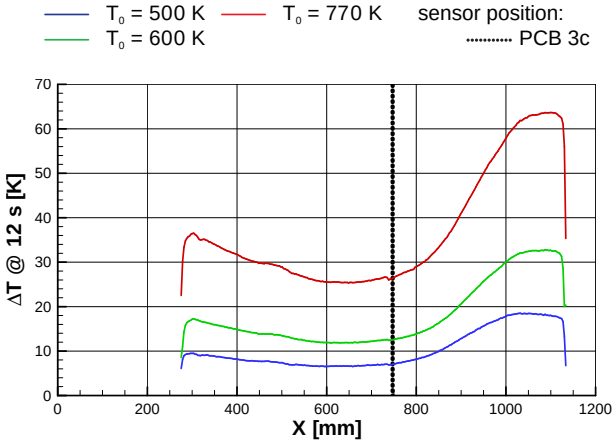

Figure 9. Temperature increase dependent on temperature @ $Ma = 6.0$, $r_N = 1.0\,\mathrm{mm}$, $Re = 4 \cdot 10^6 \frac{1}{\mathrm{m}}$, plain

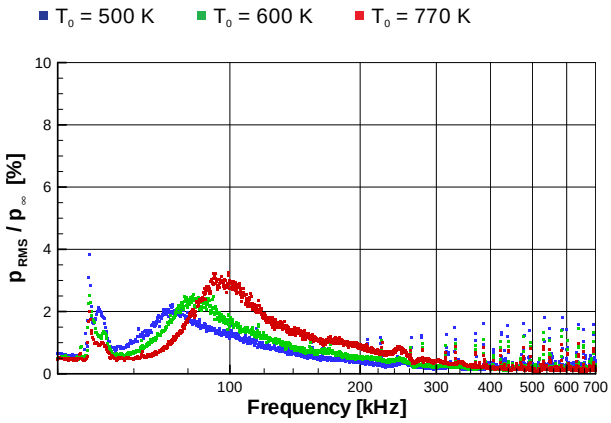

Figure 10. Pressure frequency spectra dependent on temperature @ $Ma = 6.0$, $r_N = 1.0\,\mathrm{mm}$, $Re = 4 \cdot 10^6 \frac{1}{\mathrm{m}}$, plain

3.4. Perforation

The effect of the porous surface was measured by replacing the middle section as a rotation of the whole model comes along with the need of an angle of attack adjustment. The experience of adjusting the yaw angle via the infrared images shows the high sensitivity of the transition position to the angle of attack. Another advantage is that the same PCB sensors are in use. But the result is that the porous surface has nearly no effect on the transition position. Figure 11 shows that it even tends to an earlier transition. Nevertheless figure 12 shows a significantly reduced amplitude of the Mack mode in the middle of the transition region. The amount of the damping is about 36%.

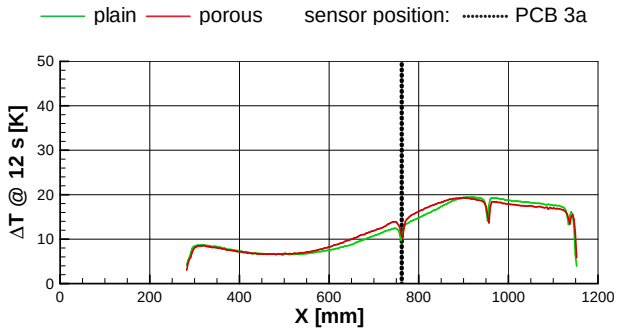

Figure 11. Temperature increase dependent on surface @ $Ma = 6.0$, $r_N = 0.15\,\mathrm{mm}$, $Re = 4 \cdot 10^6\,\frac{1}{\mathrm{m}}$, $T_0 = 500\,\mathrm{K}$

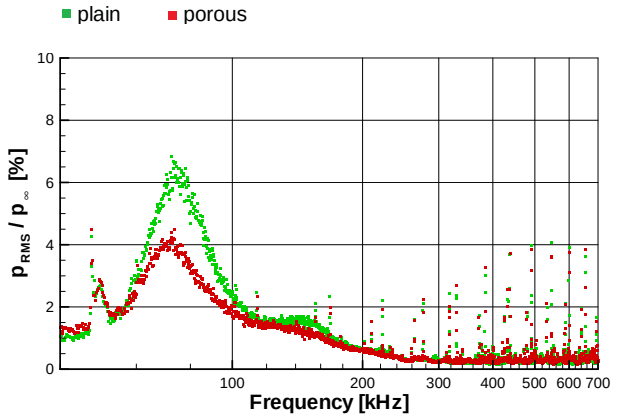

Figure 12. Pressure frequency spectra dependent on surface @ $Ma = 6.0$, $r_N = 0.15\,\mathrm{mm}$, $Re = 4 \cdot 10^6\,\frac{1}{\mathrm{m}}$, $T_0 = 500\,\mathrm{K}$

4. CONCLUSION

The results of the Reynolds number, nose radius and temperature variations concerning the transition position met the expectations and agree with former investigations as from Müller and Henckels [3]. An increase of the Reynolds number or a decrease of the nose radius shortens the transition region and moves it upstream. A change of the temperature level in the examined range has no effect on the transition. A delay of the transition due to the porous surface as observed by Rasheed et al. [5] could not be measured.

More interesting are the measured pressure frequency spectra. The Mack mode is detectable before the transition process starts and its amplitude increases to maximum within the transition region. It becomes completely destructed with the completion of the transition process. With increasing path length the frequency of the Mack mode decreases. When the Mack mode is strongly amplified a second peak forms at about twice the frequency of the main peak, and thus can be identified as its 1^{st} harmonic. These effects are also visible in the measurements of Roediger et al. [6] and Berridge et al. [1]. The increase of the Mack mode's frequency with the Reynolds number also agrees to the results of Berridge. The influence of the nose radius on the Mack mode has to be interpreted carefully. The results indicate that the Mack mode develops just with small nose radii and an increase of the nose radius reduces its frequency. The increase of the frequency with the temperature is self-evident and quantitative matches the increase of the speed of sound with the root of the temperature. Although the amplitude increase is small it has been confirmed with other experiments using a nose radius of $0.15\,\mathrm{mm}$.

Although the transition delay could not be measured, the damping of the Mack mode with the help of a regular porous surface could be verified. The amount of damping is in good agreement with the calculations done by Wartemann et al. [10].

For a more detailed investigation of the amplification and destruction of the Mack mode it would be interesting to increase the number of PCB sensors in a row. To verify the experience of Rasheed et al. [5], which show that a transition delay requires lower Reynolds numbers, a porous rear segment is needed as the transition region moves downstream. Experiments at other Mach numbers could generalize the results.

ACKNOWLEDGMENTS

These experiments are part of the DLR research project IMENS-3C. Special thanks go to Mr. Brajdic from the ILT in Aachen for his great personal commitment for the realization of the porous surface. Thanks also to PJK in Sankt Augustin for accepting the challenge of turning a sharp 3° nose. Last but not least the commitment of the technical staff of the H2K is gratefully acknowledged.

REFERENCES

[1] Berridge, D. C., Casper, K. M., Rufer, S. J., Alba, C. R., Lewis, D. R., Beresh, S. J., and Schneider, S. P. (2010). Measurements and Computations of Second-Mode Instability Waves in Three Hypersonic Wind

Tunnels. In *40th Fluid Dynamics Conference and Exhibit*, AIAA, Chicago. American Institute of Aeronautics and Astronautics.

[2] Fedorov, A. V., Shiplyuk, A. N., Maslov, A. A., Burov, E. V., and Malmuth, N. D. (2003). Stabilization of a hypersonic boundary layer using an ultrasonically absorptive coating. *Journal of Fluid Mechanics*, 479:99–124.

[3] Müller, L. and Henckels, A. (1997). Visualization of High Speed Boundary Layer Transition with FPA Infrared Technique. In *Notes on Numerical Fluid Mechanics*, volume 60, pages 245–252.

[4] Niezgodka, F.-J. (2001). *Der Hyperschallwindkanal H2K des DLR in Köln-Porz (Stand 2000)*. DLR-Mitteilungen. Deutsches Zentrum für Luft- und Raumfahrt e. V., Köln.

[5] Rasheed, A., Hornung, H. G., Fedorov, A. V., and Malmuth, N. D. (2002). Experiments on Passive Hypervelocity Boundary-Layer Control Using an Ultrasonically Absorptive Surface. *AIAA Journal*, 40(3):481–489.

[6] Roediger, T., Knauss, H., Estorf, M., Schneider, S. P., and Smorodsky, B. V. (2009). Hypersonic Instability Waves Measured Using Fast-Response Heat-Flux Gauges. *Journal of Spacecraft and Rockets*, 46(2):266–273.

[7] Walther, K., Brajdic, M., Kelbassa, I., and Poprawe, R. (2008). Bohren mit gepulster Laserstrahlung. *wt Werkstattstechnik online*, 98(6):520–523.

[8] Wartemann, V. and Lüdeke, H. (2010). Investigation of Slip Boundary Conditions of Hypersonic Flow over Microporous Surfaces. In Pereira, J. C. F. and Sequeira, A., editors, *V European Conference on Computational Fluid Dynamics*, number June, Lisbon.

[9] Wartemann, V., Lüdeke, H., and Sandham, N. D. (2009). Stability analysis of hypersonic boundary layer flow over microporous surfaces. In *16th AIAA/DLR/DGLR International Space Planes and Hypersonic Systems and Technologies Conference*, pages 1–10.

[10] Wartemann, V., Lüdeke, H., Willems, S., and Gülhan, A. (2011). Stability Analyses and Validationof a Porous Surface Boundary Condition by Hypersonic Experiments on a Cone Model. In *7th European Aerothermodynamics Symposium*, Brugge. ESA Publications Division.